2021 International Conference on Localization and GNSS (ICL-GNSS) | 978-1-7281-9644-2/20/$31.00 ©2021 IEEE | DOI: 10.1109/ICL-GNSS51451.2021.9452297

Performance Limits and Benefits of Adaptive Autoregressive Kalman Filters for GNSS Scintillation-Robust Carrier Tracking

Sergi Locubiche-Serra, Gonzalo Seco-Granados, José A. López-Salcedo
Department of Telecommunications and Systems Engineering
Universitat Autònoma de Barcelona (UAB), IEEC-CERES, Spain
Email: sergi.locubiche@uab.cat, gonzalo.seco@uab.cat, jose.salcedo@uab.cat

***Abstract*—The expansion of Global Navigation Satellite Systems (GNSS) to safety-critical applications in Equatorial and high-latitude regions has unveiled the need to cope with the so-called ionospheric scintillation, an impairment introducing rapid power and carrier phase fluctuations onto the received signal. At carrier tracking level, the use of hybrid autoregressive Kalman filter (KF-AR)-based techniques has shown great potential in mitigating its impact onto the performance of GNSS receivers. In this paper we provide a deep analysis for Kalman filter designers to have a clear idea on the interplay of the Kalman modeling parameters onto the steady-state behaviour of these techniques. To this end, we employ the Bayesian Cramér-Rao bound (BCRB) as a useful tool to predict the expected performance of KF-AR techniques in a straightforward manner. Furthermore, we evaluate the goodness of these techniques under stringent working conditions, where the BCRB analysis is further complemented with empirical results, and we show the importance of using adaptive KF-AR implementations to attain optimal performance.**

I. Introduction

Global Navigation Satellite Systems (GNSS) are considered to be one of the quintessential technologies for ubiquitous positioning and navigation purposes using satellite ranging signals. Thanks to its success in open-sky environments, plenty of efforts are shortly being made to expand this technology beyond the limits of its original design [1]. This implies moving to the arena of high-precision, safety-critical applications such as aviation, maritime navigation and autonomous vehicle driving, just to mention a few. In that sense, an upward trend is to exploit carrier phase measurements, as they are of better quality than pseudorange measurements and do provide ultra-precise positioning information. However, this goes hand in hand with new technological challenges to be faced by next-generation GNSS receivers, such as weak signal reception and multipath [2]. In particular, the deployment of GNSS in emerging countries has motivated the need to face the challenge posed by the so-called ionospheric scintillation.

Ionospheric scintillation is one of the most challenging sources of error to combat within the GNSS community [3]. It is an impairment whereby transionospheric radio wave propagation is influenced by solar radiation ionizing the upper Earth's atmosphere. The ionospheric electron density irregularities affect GNSS signals in form of random amplitude fades and rapid phase fluctuations, causing severe carrier phase jitter and loss of signal, and thus having a detrimental effect onto the performance of GNSS receivers. Moreover, ionospheric scintillation is known to be more frequent in Equatorial and high-latitude regions [4], thus hampering the deployment of GNSS in those areas. Interestingly, the bottleneck of GNSS receivers under scintillation conditions takes place in the determination of the user dynamics phase of interest at carrier tracking level. Therefore, the design of advanced carrier tracking techniques for providing dynamics phase measurements robust to ionospheric scintillation becomes of paramount importance.

Traditional carrier tracking architectures implement the well-known phase-locked loop (PLL), a closed-loop architecture that is known to have serious issues in the presence of propagation impairments such as ionospheric scintillation. As a countermeasure, by noting that the random nature of the latter can be modeled through correlated Gaussian functions, such as autoregressive (AR) processes [5], the so-called hybrid autoregressive Kalman filter (KF-AR) arises as the natural leap forward for estimating the user dynamics phase in the presence of scintillation. It is an innovative approach pioneered by the authors of this work [6], [7] that embeds the dynamics phase and scintillation phase signal models into one single state-space formulation. In [6], a leap forward was made by proposing a fully adaptive KF-AR implementation in order to deal with the time-varying nature of ionospheric scintillation. In this way, clean (*i.e.* undisturbed) estimates of the user dynamics phase can be provided, while making the presence of time-varying scintillation explicit.

The use of KF-AR-based techniques has shown great potential to deal with ionospheric scintillation in GNSS receivers [8], [9]. However, the literature still lacks a deep analysis on the interplay of the Kalman modeling parameters playing a key role in the filtering performance, thus preventing Kalman filter designers from fully understanding the behaviour of these techniques. Furthermore, existing contributions so far have, to our best, proven the effectiveness of the KF-AR only in controlled scenarios with favorable signal reception conditions. Therefore, this paper intends to contribute in a twofold way. On the one hand, to shed light on the steady-state behaviour of KF-AR techniques as a function of the AR modeling parameters, so that designers can have a clear idea during the design and tuning processes. To this end, we will make use of the Bayesian Cramér-Rao bound (BCRB), a useful

This work has been supported by the Spanish Ministry of Economy and Competitiveness under grant TEC2017-89925-R.

tool to predict the best achievable estimation performance as a function of the Kalman configuration parameters. And, on the other hand, to evaluate the performance of KF-AR techniques over conventional PLLs under stringent working conditions, and to reaffirm the importance of using adaptive implementations over fixed ones. For this purpose, we will extend the analysis in previous contributions by considering different realistic receiver noise (assumed additive white Gaussian, AWGN) hypotheses, from open-sky environments to urban scenarios with abounding obstacles to the line-of-sight satellite visibility, and we will complement the analysis with some empirical results for the sake of completeness.

II. Statement of Problem and Signal Model

A. State-Space Model for Dynamics Phase

The discrete-time evolution of the dynamics phase of interest, denoted as $\theta(n)$, can be approximated by a third-order kinematic model [10] as follows,

$$\theta(n) \approx \theta(n-1) + T\dot{\theta}(n-1) + \frac{T^2}{2}\ddot{\theta}(n-1) + \frac{T^3}{3!}\dddot{\theta}(n-1) \quad (1)$$

with T the sampling time, and where $\dot{\theta}(n)$, $\ddot{\theta}(n)$ and $\dddot{\theta}(n)$ are the Doppler shift, Doppler rate and Doppler acceleration, respectively (*i.e.* first, second and third derivatives of $\theta(n)$).

In terms of Kalman filtering, the model in (1) can be written in state-space notation as the state transition equation,

$$\mathbf{x}_\theta(n) = \begin{bmatrix} 1 & 1 & 1/2 \\ 0 & 1 & 1 \\ 0 & 0 & 1 \end{bmatrix} \mathbf{x}_\theta(n-1) + \begin{bmatrix} 1/6 \\ 1/2 \\ 1 \end{bmatrix} v(n) \quad (2)$$

$$\mathbf{x}_\theta(n) = \mathbf{F}_\theta \mathbf{x}_\theta(n-1) + \mathbf{G}_\theta v(n) \quad (3)$$

where $\mathbf{x}_\theta(n) \doteq \left[\theta(n) \quad T\dot{\theta}(n) \quad T^2\ddot{\theta}(n)\right]^T$ is the well-known state vector containing the sample functions of the dynamics phase, and $\mathbf{F}_\theta$ is the transition matrix used to propagate the state vector over time. The parameter $v(n) \doteq T^3\dddot{\theta}(n)$ stands for some process noise accounting for the higher-order terms of the signal model missing in $\mathbf{x}_\theta(n)$, and it can be modeled as $v(n) \sim \mathcal{N}(0, \sigma_v^2)$, with $\mathrm{E}[v(i)\, v^*(j)] = 0$ for $i \neq j$. In that sense, $\mathbf{G}_\theta$ is the process noise matrix in charge of weighting the effect of $v(n)$ onto each state.

B. State-Space Model for Scintillation Phase

On the other hand, the discrete-time evolution of scintillation phase, denoted as $\psi(n)$, is considered to follow a *p*th-order autoregressive process, usually expressed as AR(*p*), given by [11],

$$\psi(n) \approx \sum_{k=1}^{p} \beta_k \psi(n-1) + s_p(n) \quad (4)$$

where $\{\beta_k\}_{k=1}^p$ are the set of p AR coefficients, and $s_p(n)$ is the so-called AR driving noise or prediction error, usually modeled as $s_p(n) \sim \mathcal{N}\left(0, \sigma_{s_p}^2\right)$, with $\mathrm{E}\left[s_p(i)\, s_p^*(j)\right] = 0$ for $i \neq j$.

In terms of Kalman filtering, the model in (4) can be written in state-space notation as the state transition equation,

$$\mathbf{x}_{\psi_p}(n) = \begin{bmatrix} \beta_1 & \beta_2 & \beta_3 & \cdots & \beta_p \\ 1 & 0 & 0 & \cdots & 0 \\ 0 & 1 & 0 & \cdots & 0 \\ \vdots & & \vdots & \ddots & \vdots \\ 0 & \cdots & 0 & 1 & 0 \end{bmatrix} \mathbf{x}_{\psi_p}(n-1) + \begin{bmatrix} 1 \\ 0 \\ 0 \\ \vdots \\ 0 \end{bmatrix} s_p(n) \quad (5)$$

$$\mathbf{x}_{\psi_p}(n) = \mathbf{F}_{\psi_p} \mathbf{x}_{\psi_p}(n-1) + \mathbf{G}_{\psi_p} s_p(n) \quad (6)$$

where $\mathbf{x}_{\psi_p}(n) \doteq \left[\psi(n) \quad \psi(n-1) \quad \cdots \quad \psi(n-p+1)\right]^T$ is the $(p \times 1)$ state-space vector of the AR(*p*) random process, and $s_p(n)$ plays the role of the Kalman process noise.

C. KF-AR State-Sace Formulation

The beauty of the KF-AR is that it embeds the model for the dynamics phase in (2) and the one for scintillation phase in (5) into one single state-space formulation, thus leading to the following augmented state transition equation,

$$\begin{bmatrix} \mathbf{x}_\theta(n) \\ \mathbf{x}_{\psi_p}(n) \end{bmatrix} = \begin{bmatrix} \mathbf{F}_\theta & \mathbf{0}_{3\times p} \\ \mathbf{0}_{p\times 3} & \mathbf{F}_{\psi_p} \end{bmatrix} \begin{bmatrix} \mathbf{x}_\theta(n-1) \\ \mathbf{x}_{\psi_p}(n-1) \end{bmatrix} + \begin{bmatrix} \mathbf{G}_\theta & \mathbf{0}_{3\times 1} \\ \mathbf{0}_{p\times 1} & \mathbf{G}_{\psi_p} \end{bmatrix} \begin{bmatrix} v(n) \\ s_p(n) \end{bmatrix} \quad (7)$$

$$\mathbf{x}(n) = \mathbf{F}\mathbf{x}(n-1) + \mathbf{G}\mathbf{u}(n) \quad (8)$$

where the state vector $\mathbf{x}(n) \doteq \left[\mathbf{x}_\theta(n) \quad \mathbf{x}_{\psi_p}(n)\right]^T$ concatenates the magnitudes of interest for carrier dynamics and scintillation phase tracking, the transition matrix $\mathbf{F}$ is a block-diagonal matrix formed by the transition matrices of each contribution, and the effect of the process noise onto the different states becomes zero-mean with covariance matrix,

$$\mathbf{Q} \doteq \begin{bmatrix} \sigma_v^2 \mathbf{G}_\theta \mathbf{G}_\theta^T & \mathbf{0}_{3\times p} \\ \mathbf{0}_{p\times 3} & \sigma_{s_p}^2 \mathbf{G}_{\psi_p} \mathbf{G}_{\psi_p}^T \end{bmatrix}. \quad (9)$$

The KF-AR aims at providing clean estimates of $\mathbf{x}(n)$ based on the noisy measurements available at its input, which are given by the following measurement equation,

$$z(n) = \theta(n) + \psi(n) + w(n) \quad (10)$$

$$z(n) = \mathbf{H}\mathbf{x}(n) + w(n) \quad (11)$$

understood as a linear transformation of the state vector $\mathbf{x}(n)$ through the observation matrix $\mathbf{H} \doteq \left[1 \quad 0 \quad 0 \quad 1 \quad \mathbf{0}_{1\times(p-1)}\right]$, and where $w(n) \sim \mathcal{N}\left(0, \sigma_w^2\right)$ accounts for the AWGN noise corrupting the measurements.

D. Recursive BCRB

The estimation performance of the Kalman filter is given by the covariance matrix of the state estimate, $\mathbf{\Sigma}_\mathbf{x}(n) \doteq \mathrm{E}\left[(\hat{\mathbf{x}}(n) - \mathbf{x}(n))(\hat{\mathbf{x}}(n) - \mathbf{x}(n))^H\right]$, which is lower bounded by the BCRB,

$$\mathbf{\Sigma}_\mathbf{x}(n) \geq \mathbf{J}_\mathrm{B}^{-1}(n) \quad (12)$$

with $\mathbf{J}_\mathrm{B}(n)$ the Bayesian information matrix (BIM) that can be computed recursively as [12],

$$\mathbf{J}_\mathrm{B}(n) = \left[\mathbf{Q} + \mathbf{F}\mathbf{J}_\mathrm{B}^{-1}(n-1)\mathbf{F}^H\right]^{-1} + \sigma_w^{-2}\mathbf{H}^H\mathbf{H}. \quad (13)$$

where the initial covariance matrix of the state estimate set by the user can be readily employed to initialise such recursion. That is, $\mathbf{J}_\mathrm{B}^{-1}(0) = \mathbf{\Sigma}_\mathbf{x}(0)$.

III. Performance Limits of KF-AR Techniques

The availability of the recursive BCRB in (13) allows one to predict the performance of KF-AR filters in a straightforward manner and extract different conclusions on how good the estimates provided by this kind of techniques are expected to be. By introducing the signal models and Kalman matrices in Section II into (13), we carry out next a detailed analysis on the steady-state behaviour (*i.e.* $n \to \infty$) of the KF-AR as a function of the different parameters used to configure the technique. To this end, in order to focus on the impact of ionospheric scintillation, in the sequel we will consider a static receiver with dynamics process noise variance $\sigma_v^2 = 3.4 \cdot 10^{-17}$ rad^2 as a result of considering a residual Doppler acceleration of $2 \cdot 10^{-4}$ Hz/s^2 due to satellite motion. For simplicity, we will henceforth refer to $\mathbf{J}_{\mathrm{B}}^{-1}\,(n \to \infty)$ as directly $\mathbf{J}_{\mathrm{B}}^{-1}$. More precisely, the BCRB for dynamics phase will be referred to as $\left[\mathbf{J}_{\mathrm{B}}^{-1}\right]_{1,1}$, and the BCRB for scintillation phase as $\left[\mathbf{J}_{\mathrm{B}}^{-1}\right]_{4,4}$.

A. BCRB for AR(1) as a Function of Model Parameters

We will start by considering an AR(1) process for scintillation phase and evaluating the impact of the AR model parameters onto the BCRB. For a carrier-to-noise ratio (C/N_0) of 45 dB-Hz, Figure 1 shows the root BCRBs, $\sqrt{\left[\mathbf{J}_{\mathrm{B}}^{-1}\right]_{1,1}}$ and $\sqrt{\left[\mathbf{J}_{\mathrm{B}}^{-1}\right]_{4,4}}$, for different values of the AR coefficient β_1 as a function of the AR driving noise $\sigma_{s_p}^2$ normalized to $4\pi^2$ rad^2. The black striped line, denoted as $\sqrt{\left[\tilde{\mathbf{J}}_{\mathrm{B}}^{-1}\right]_{1,1}}$, depicts the dynamics phase root BCRB when scintillation is absent. As can be observed, increasing either β_1 or $\sigma_{s_p}^2$ induces a higher root BCRB, departing from $\sqrt{\left[\tilde{\mathbf{J}}_{\mathrm{B}}^{-1}\right]_{1,1}}$ when these values are sufficiently large. Intuitively, this phenomenon can be understood in two ways, although linked with one another. First, by thinking of the KF-AR as a conventional PLL with some equivalent loop bandwidth that is interestingly determined by the Kalman process noise [13], in this case $\sigma_{s_p}^2$. As scintillation gains relevance, the KF-AR must enlarge its equivalent loop bandwidth in order to follow scintillation fluctuations, which means less noise filtering capabilities in contrast, and thus a larger BCRB. And second, by noticing that larger $\sigma_{s_p}^2$ means more discrepancies between the KF-AR model and the actual scintillation phase model, thus eventually degrading the estimation performance.

When scintillation errors lose relevance and the model discrepancies tend to zero (that is, $\sigma_{s_p}^2 \to 0$), $\sqrt{\left[\mathbf{J}_{\mathrm{B}}^{-1}\right]_{4,4}}$ decreases without bound, regardless of the value of β_1. This is because, in this situation, scintillation phase can be perfectly estimated, and thus it can perfectly be subtracted from the input signal, consequently improving the estimation performance of the dynamics phase. This is equivalent to a scintillation-free situation, where the KF-AR becomes a standard KF that only deals with dynamics phase, and thus the corresponding root BCRB attains $\sqrt{\left[\tilde{\mathbf{J}}_{\mathrm{B}}^{-1}\right]_{1,1}}$, which exhibits a floor saturation effect due to the presence of non-zero dynamics process noise [12] denoting discrepancies in the Kalman model. This latter behaviour can be understood as the KF with an equivalent loop bandwidth large enough to keep the filter aware of possible variations in the input carrier phase dynamics that, conversely, poses a limit on the estimation performance.

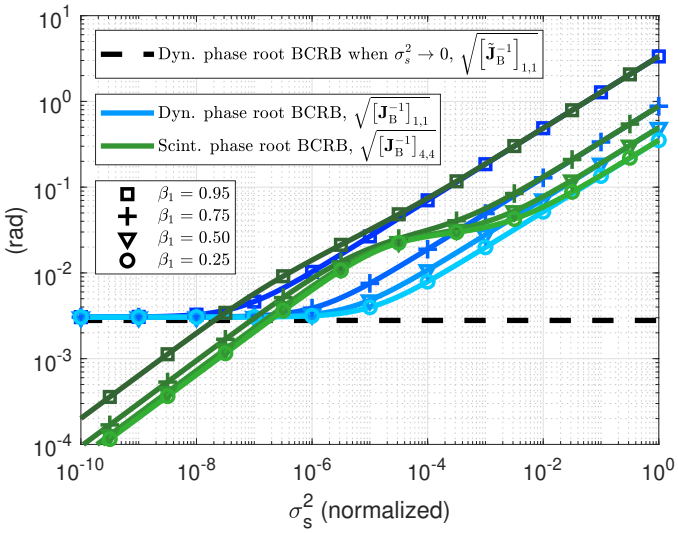

Fig. 1: Carrier dynamics and scintillation phase root BCRB as a function of β_1 and $\sigma_{s_p}^2$.

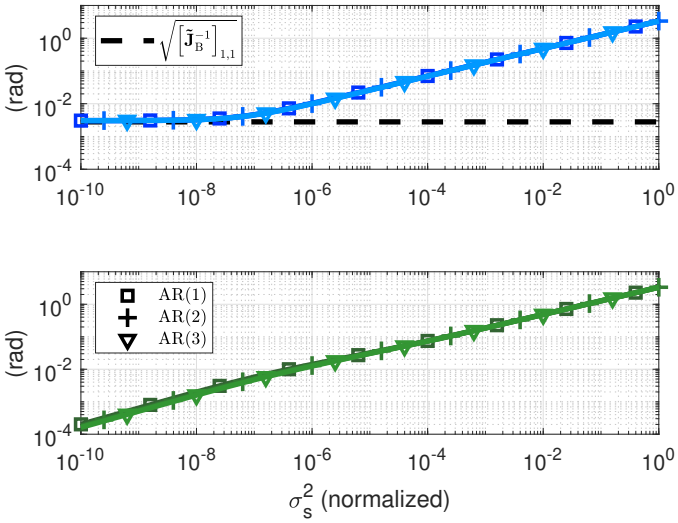

Fig. 2: (Top) Carrier dynamics and (bottom) scintillation phase root BCRB as a function of $\sigma_{s_p}^2$, for different AR model orders.

B. BCRB as a Function of AR Model Order

We now evaluate the impact of the AR model order onto the BCRB. For the same environmental conditions as in figure 1, figure 2 shows the the root BCRBs $\sqrt{\left[\mathbf{J}_{\mathrm{B}}^{-1}\right]_{1,1}}$ and $\sqrt{\left[\mathbf{J}_{\mathrm{B}}^{-1}\right]_{4,4}}$ considering different AR model orders, from 1 to 3. As can be observed, whereas using higher model orders may provide a better fit of the AR models to correlated scintillation phase fluctuations, their impact on the best achievable performance is practically non-existent, as long as the sum of the $\{\beta_k\}_{k=1}^{p}$ coefficients is the same for all model orders. The sum of the coefficients must be smaller than 1 to ensure that the filter is stable. In figure 2, it is considered that $\sum_{k=1}^{p} \beta_k = 0.95$. If the sum of the β_p coefficients differs from 0.95, the BCRB follows the fashion of previous figure 1.

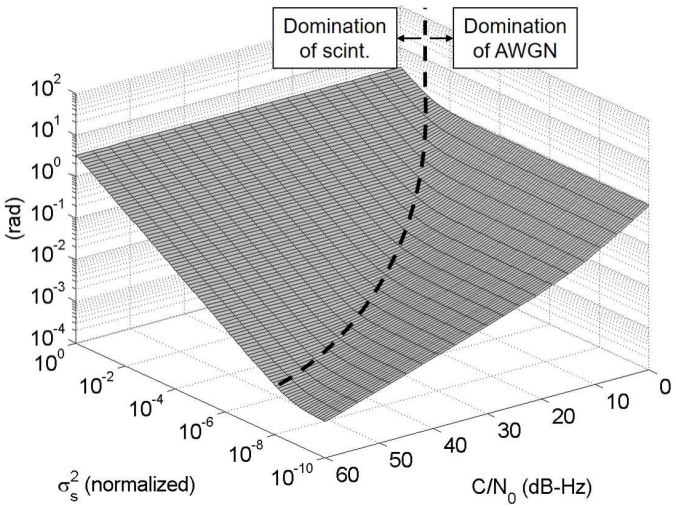

Fig. 3: 3-D plot depicting dynamics phase root BCRB as a function of $\sigma^2_{s_p}$ and C/N_0.

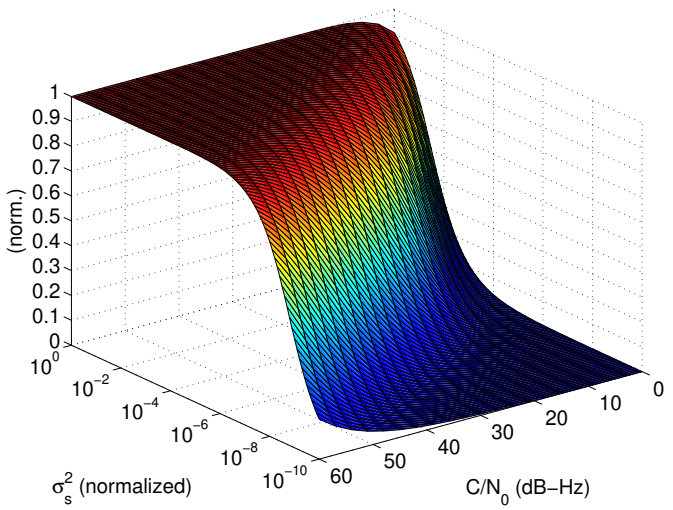

Fig. 4: Coupling factor between dynamics phase and scintillation phase as a function of $\sigma^2_{s_p}$ and C/N_0.

C. BCRB as a Function of C/N_0

We now extend the analysis to contemplate multiple C/N_0 conditions, depicting from open-sky environments to urban scenarios with obstacles degrading signal reception. Figure 3 shows a two-dimensional analysis of $\sqrt{\left[\mathbf{J}_{\mathrm{B}}^{-1}\right]_{1,1}}$ as a function of $\sigma^2_{s_p}$ and the C/N_0. As expected, for very small values of $\sigma^2_{s_p}$ (*i.e.* in the absence of scintillation), the BCRB depends fully on the C/N_0, as the KF-AR resembles a standard, non-AR KF, and the phase jitter decreases for larger C/N_0. As $\sigma^2_{s_p}$ increases, the BCRB also starts increasing, as already explained in figure 1. Here, a higher scintillation noise induces higher errors in the estimated scintillation, with the BCRB diverging from $\left[\tilde{\mathbf{J}}_{\mathrm{B}}^{-1}\right]_{1,1}$. However, as C/N_0 decreases, scintillation has to be more powerful (*i.e.* larger $\sigma^2_{s_p}$) to start dominating over noise on the dynamics phase.

This latter phenomenon leads one to think that, when working at low C/N_0, AWGN produces a masking effect over scintillation, meaning that scintillation falls below the noise level, and the dynamics phase is dependent only on the effect of AWGN. This is applicable when $\sqrt{\left[\mathbf{J}_{\mathrm{B}}^{-1}\right]_{1,1}}$ remains flat when moving along $\sigma^2_{s_p}$ for a fixed value of C/N_0. As previously stated, this is equivalent to a scintillation-free situation. On the other hand, scintillation is the predominant effect over measurement noise when $\sqrt{\left[\mathbf{J}_{\mathrm{B}}^{-1}\right]_{1,1}}$ remains flat when moving along the C/N_0 for a fixed value of $\sigma^2_{s_p}$. In figure 3, the black striped line illustrates the boundary between AWGN predominance and scintillation predominance.

D. Coupling between Dynamics and Scintillation Phases

The particularity of the KF-AR is that it estimates not only the carrier phase dynamics, but also the fluctuating scintillation phase. Hence, depending on the working conditions, both estimates are coupled to more or less extent. That is, the estimates of dynamics phase are limited by the errors in the estimation of scintillation phase. In contrast to the input measurement noise, which is aimed to be filtered out, the scintillation phase is a noise-like disturbance aimed to be estimated, and thus the estimates will inevitably present some error. As a consequence, a portion of scintillation phase remains after mitigation, which eventually propagates to the estimated dynamics phase.

This phenomenon can readily be inferred from figure 1. In there, $\left[\mathbf{J}_{\mathrm{B}}^{-1}\right]_{4,4}$ increases linearly as the scintillation prediction noise also increases. However, the point when $\left[\mathbf{J}_{\mathrm{B}}^{-1}\right]_{1,1}$ starts diverging from $\left[\tilde{\mathbf{J}}_{\mathrm{B}}^{-1}\right]_{1,1}$ coincides with a change in the slope of $\left[\mathbf{J}_{\mathrm{B}}^{-1}\right]_{4,4}$. At this point, scintillation phase starts having an impact onto $\left[\mathbf{J}_{\mathrm{B}}^{-1}\right]_{1,1}$. The estimation of user phase and scintillation phase starts being coupled, and this effect increases until the user phase performance is fully captured by $\left[\mathbf{J}_{\mathrm{B}}^{-1}\right]_{4,4}$.

The effect can also be observed in figure 3. Dynamics phase and scintillation phase start being coupled above the black striped line, which coincides with the point that determines when ionospheric scintillation is predominant over AWGN. As the C/N_0 decreases, a larger $\sigma^2_{s_p}$ is needed for scintillation to predominate over noise, for the coupling effect to take place. On the other hand, figure 4 depicts the coupling factor between dynamics phase and scintillation phase, determined as the ratio between the cross-covariance and dynamics phase estimation variance elements in the steady-state covariance matrix of the state estimate. That is, $\left[\mathbf{\Sigma}_{\mathbf{x}}\left(n\rightarrow\infty\right)\right]_{4,1} / \left[\mathbf{\Sigma}_{\mathbf{x}}\left(n\rightarrow\infty\right)\right]_{1,1}$. The coupling factor is valued between 0 meaning no coupling at all, and 1 meaning full coupling between the estimates of both magnitudes. As can be observed, the black striped line in figure 3 coincides with the point in figure 4 when the coupling factor starts augmenting. Hence, the same conclusion can be extracted from figure 4. For high C/N_0, dynamics phase and scintillation phase estimates start being coupled at very small $\sigma^2_{s_p}$, whereas for low C/N_0, the scintillation prediction error $\sigma^2_{s_p}$ has to be larger for this to occur.

IV. Benefits of Adaptive KF-AR Techniques

The objective of this section is twofold. On the one hand, to show the importance of employing adaptive KF-AR implementations to deal with time-varying working conditions in a

realistic environment. On the other hand, to use the BCRB tool to evaluate the expected behaviour of such techniques under different scintillation intensities, namely moderate and severe, and received signal conditions. To this end, we will focus on the adaptive approach introduced in [6], the termed AHL-KF-A2R(p), where the authors of this work proposed three independent adaptive implementations. First, a real-time estimation of the AR model parameters, $\{\beta_k\}_{k=1}^{p}$ and $\sigma_{s_p}^2$, using the Yule-Walker equations [11] in an online manner. Second, a real-time estimation of the optimal AR model order using the minimum description length (MDL) criterion [14]. And third, an adaptive, hard-limited (AHL) Kalman measurement noise variance based on actual C/N_0 measurements to deal with the non-linear signal amplitude fades introduced by scintillation, particularly severe scintillation. The beauty of this approach is not only that it exploits the information on the actual C/N_0, but also that it establishes a C/N_0 threshold below which the KF-AR is forced to disconnect the input measurements. By doing so, the Kalman filter is protected from abnormal deep fades in the C/N_0, and relies only on its internal state-space model until the C/N_0 recovers to nominal conditions. In this work, the threshold is set to $C/N_0 = 25$ dB-Hz.

A. Cornell Scintillation Model

In the sequel, we will consider a class of scintillation data generated through the so-called Cornell Scintillation Model (CSM). It synthesizes scintillation time series using an index S_4 as an indicator of scintillation intensity, and τ_0 as the decorrelation time of consecutive scintillation samples [5]. As a rule of thumb, the larger S_4 and smaller τ_0, the more severe scintillation. For moderate scintillation, we will consider $\{S_4 = 0.5,\ \tau_0 = 0.8\ \text{s}\}$, leading to a scintillation phase with standard deviation $\sigma_\psi = 0.3$ rad, whereas for severe scintillation, we will consider $\{S_4 = 0.8,\ \tau_0 = 0.4\ \text{s}\}$, leading to a scintillation phase with standard deviation $\sigma_\psi = 0.8$ rad.

B. Seeking KF-AR Optimal Performance

We start the analysis by focusing on the presence of CSM severe scintillation as the most critical situation faced by a GNSS receiver. In that sense, the top plot of figure 5 depicts the operational range of non-AHL and AHL adaptive KF-AR techniques in terms of $\sqrt{\left[\mathbf{J}_{\text{B}}^{-1}\right]_{1,1}}$ and $\sqrt{\left[\mathbf{J}_{\text{B}}^{-1}\right]_{4,4}}$, as a function of the nominal C/N_0. The figure also includes the empirical root mean square error (RMSE) of 100 Monte Carlo realizations of the techniques. This is done in order to evaluate the goodness of each technique in terms of the closeness to the BCRB. On the other hand, the bottom plot of figure 5 shows the empirical probability of losing track of the signal.

As the interest lies in tracking carrier phase dynamics, in this analysis we will mainly focus on the carrier phase dynamics estimation performance. It can be seen that the RMSE of the KF-A2R(p) technique follows the shape of $\sqrt{\left[\mathbf{J}_{\text{B}}^{-1}\right]_{1,1}}$, although it presents some gap. Such effect is caused by the presence of deep fades under severe scintillation conditions, which are not dealt with by the KF-A2R(p), thus preventing the dynamics phase RMSE from attaining optimal performance. The deep fades also have an impact on the probability of loss-of-lock. The effect of higher loss-of-lock

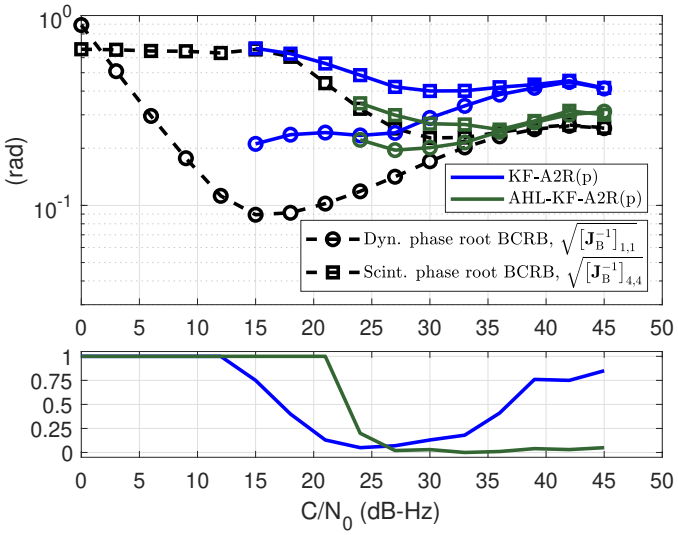

Fig. 5: (Top) Root BCRB and empirical RMSE of KF-AR techniques as a function of C/N_0. (Bottom) probability of loss-of-lock.

for larger C/N_0 is caused by the fact that, when AWGN becomes more negligible, the deep fades become more relevant to the KF. On the other hand, at high C/N_0, the dynamics phase and scintillation phase RMSE present very similar values, due to the high coupling under these conditions.

The AHL-KF-A2R(p) presents smaller operational range than the non-AHL technique (C/N_0 of 25 dB-Hz against 15 dB-Hz), which is due to the hard-limiting threshold itself. Nonetheless, the AHL condition is shown to provide attractive advantages. First, the dynamics phase RMSE is smaller than in the KF-A2R(p) and fully reaches the performance lower bound given by the BCRB. This is because the BCRB accounts for nominal C/N_0 values, in an ideal situation with no signal power fades. Therefore, the AHL implementation filters such fades and counteracts their effect onto the effective C/N_0, thus eventually attaining optimal performance. And second, the AHL-KF-A2R(p) benefits from a significantly smaller probability of loss-of-lock, thus ensuring service availability under severe scintillation conditions.

In the top plot of figure 5, $\left[\mathbf{J}_{\text{B}}^{-1}\right]_{1,1}$ exhibits a valley effect at C/N_0 around 15 dB-Hz. In line with the previous conclusions, AWGN is the predominant effect in these circumstances, and thus the BCRB decreases as the C/N_0 increases until 15 dB-Hz. Then, at $C/N_0 \geq 15$ dB-Hz, scintillation starts gradually gaining relevance over noise, thus being beneficial for the estimation of scintillation as $\left[\mathbf{J}_{\text{B}}^{-1}\right]_{4,4}$ decreases until stabilizing above 30 dB-Hz. At this point, the scintillation phase BCRB experiences a floor saturation effect, which is conceptually similar to that with dynamics given by $\left[\tilde{\mathbf{J}}_{\text{B}}^{-1}\right]_{1,1}$. However, the coupling effect is again observed to impact onto $\left[\mathbf{J}_{\text{B}}^{-1}\right]_{1,1}$, as the latter increases along with the C/N_0, above 15 dB-Hz, and the estimation performance is eventually captured by the errors in the estimated scintillation phase. In addition, the probability of loss-of-lock degrades as well when deep fades start rising above the noise level in the KF-A2R(p),

where these are not filtered. Based on these observations, the importance of using the AHL implementation is concluded.

C. Importance of Using Adaptive KF-AR Techniques

Once confirmed that the AHL-KF-A2R(p) can attain optimal performance, we can make use of the BCRB tool to stand out the importance of using adaptive KF-AR implementations over fixed ones. In that sense, figure 6 compares the term $\sqrt{\left[\mathbf{J}_{\mathrm{B}}^{-1}\right]_{1,1}}$ between a KF-AR with fixed parameters and the AHL-KF-A2R(p), for both CSM moderate and severe scintillation. The root BCRB of the AHL-KF-A2R(p) corresponds to that already depicted in figure 5. For the sake of completeness, figure 6 also depicts the best achievable performance that would be attained by conventional PLLs in the presence of ionospheric scintillation.

The outperformance of adaptive techniques is confirmed under both moderate and severe scintillation, particularly if compared to the expected PLL performance, which is ultimately limited by the standard deviation of the scintillation time series under study as it estimates scintillation phase as part of the user dynamics. At low-to-mid C/N_0, in the range of [10, 30] dB-Hz, the shape of the KF-AR BCRB is quite different between fixed and adaptive. In this range of C/N_0, the root BCRB is smaller in the case of adaptive KF-AR implementations, with an improvement of 0.15 rad to below 0.1 rad for moderate scintillation, and 0.25 rad to 0.1 rad for severe scintillation. This behaviour stands out the fact that, when AWGN is the predominant effect over scintillation, not only there is no need for the KF-AR to activate the AR part, but doing so even becomes harmful to the estimation performance. That is, using the AR module unnecessarily in the KF-AR incurs in some performance degradation as scintillation gradually falls below the noise level. In contrast, the adaptive implementations of the AHL-KF-A2R(p) technique automatically disable the AR part when not needed, either by estimating zero AR coefficients or by readily introducing a zero-th AR model order. Based on these observations, the importance of using adaptive KF-AR implementations over fixed ones is concluded.

V. Conclusion

This paper has provided a deep insight into the performance of GNSS carrier tracking under the presence of ionospheric scintillation using KF-AR techniques. Two main contributions have been made. First, a qualitative analysis on the interplay of the KF-AR modeling parameters and signal reception conditions playing a key role in the estimation performance of carrier phase dynamics. The BCRB has revealed a coupling effect by which the dynamics phase estimation is limited by the errors in the estimated scintillation phase, although clearly outperforming conventional PLLs. And second, we have confirmed the importance of using adaptive KF-AR techniques to attain optimal performance under stringent working conditions by self-adjusting the AR module when AWGN gradually gains relevance. The AHL has proven to become of paramount importance to counteract the deep fades introduced by scintillation. The work presented in this paper has been intended to serve as a useful guideline for a better understanding on the behaviour of the KF-AR in realistic environments.

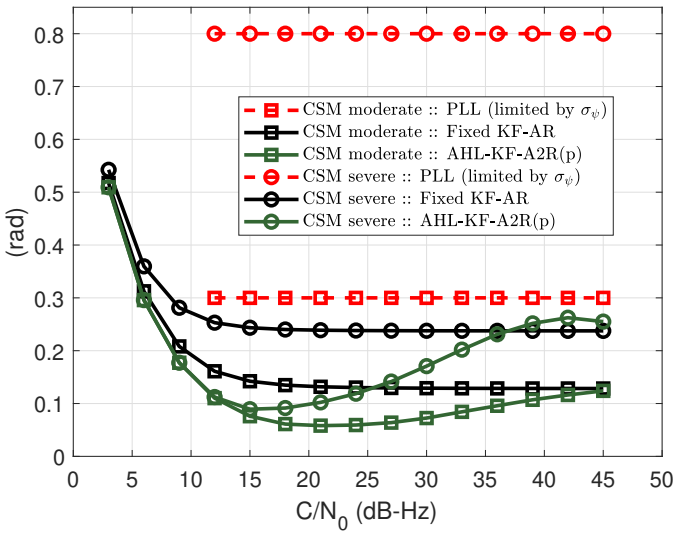

Fig. 6: Best achievable dynamics phase estimation performance when using a fixed KF-AR implementation versus the adaptive AHL-KF-A2R(p) versus conventional PLL.

References

[1] European GNSS Agency (GSA), "GNSS Market Report, Issue 6," Oct 2019.

[2] G. Seco-Granados, J. López-Salcedo, D. Jiménez-Baños, and G. López-Risueño, "Challenges in Indoor Global Navigation Satellite Systems: Unveiling its core features in signal processing," *IEEE Signal Processing Magazine*, vol. 29, no. 2, pp. 108–131, 2012.

[3] J. Lee, Y. T. J. Morton, J. Lee, H. Moon, and J. Seo, "Monitoring and Mitigation of Ionospheric Anomalies for GNSS-Based Safety Critical Systems: A review of up-to-date signal processing techniques," *IEEE Signal Processing Magazine*, vol. 34, no. 5, pp. 96–110, 2017.

[4] P. M. Kintner, T. E. Humphreys, and J. Hinks, "GNSS and ionospheric scintillation. How to survive the next solar maximum," *Inside GNSS*, vol. 4, no. 4, pp. 22–30, Jul 2009.

[5] T. E. Humphreys, M. L. Psiaki, B. M. Ledvina, A. P. Cerruti, and P. M. Kintner, "A Data-Driven Testbed for Evaluating GPS Carrier Tracking Loops in Ionospheric Scintillation," *IEEE Transactions on Aerospace and Electronic Systems*, vol. 46, no. 4, pp. 1609–1623, 2010.

[6] S. Locubiche-Serra, G. Seco-Granados, and J. A. López-Salcedo, "Doubly-adaptive autoregressive Kalman filter for GNSS carrier tracking under scintillation conditions," *2016 International Conference on Localization and GNSS (ICL-GNSS)*, pp. 1–6, Jun 2016.

[7] J. Vilà-Valls, J. A. López-Salcedo, and G. Seco-Granados, "An interactive multiple model approach for robust GNSS carrier phase tracking under scintillation conditions," *2013 IEEE International Conference on Acoustics, Speech and Signal Processing (ICASSP)*, pp. 6392–6396, May 2013.

[8] F. Fohlmeister, F. Antreich, and J. Nossek, "Dual Kalman filtering based GNSS phase tracking for scintillation mitigation," pp. 1151–1158, 2018.

[9] Y. Morton, F. Van Diggelen, J. Spilker, B. Parkinson, S. Lo, and G. Gao, *Position, Navigation, and Timing Technologies in the 21st Century. Volumes 1 and 2: Integrated Satellite Navigation, Sensor Systems, and Civil Applications*. John Wiley and Sons, 2020.

[10] Y. B. Shalom, X. R. Li, and T. Kirubarajan, *Estimation with Applications to Tracking and Navigation: Theory Algorithms and Software*. New York, NY, USA: Wiley, 2001.

[11] S. M. Kay, *Fundamentals of Statistical Signal Processing: Estimation Theory*. Upper Saddle River, NJ, USA: Prentice-Hall, 1993.

[12] H. L. V. Trees and K. L. Bell, *Bayesian Bounds for Parameter Estimation and Nonlinear Filtering/Tracking*. New York, NY, USA: Wiley, 2007.

[13] D. J. Jwo, "Optimization and sensitivity analysis of GPS receiver tracking loops in dynamic environments," *IET Proceedings on Radar, Sonar and Navigation*, vol. 148, pp. 241–250, Sep 2001.

[14] P. M. Djuric, S. M. Kay, K. M. Vijay, and B. W. Douglas, "Spectrum estimation and modeling," *Digital Signal Processing Handbook, CRC Press*, 1999.